Long-Lived Charge-Transfer Excitons in a Graphene-PTCDI-TiOPc Trilayer Heterostructure

Ryan J. Scott, Neno Fuller, Adithya Sadanandan, Pavel Valencia-Acuna, Wai-Lun Chan, Qunfei Zhou,* and Hui Zhao*

Department of Physics and Astronomy, The University of Kansas, Lawrence, Kansas 66045, United States

E-mail: qunfei.zhou@ku.edu; huizhao@ku.edu

Abstract

Excitation transfer across the interfaces between graphene, perylenetetracarboxylic diimide (PTCDI), and titanyl phthalocyanine (TiOPc) was studied using transient absorption and photoluminescence spectroscopy. Both photoluminescence quenching and transient absorption measurements confirm the presence of a type-II interface between PTCDI and TiOPc. While the graphene/PTCDI interface is expected to exhibit type-I behavior, transient absorption measurements indicate that only electrons transfer from PTCDI to graphene, with no evidence of hole transfer. Density functional theory calculations reveal significant ground-state electron transfer from graphene to PTCDI, resulting in band bending that prevents excited holes from transferring from PTCDI to graphene. This feature is exploited in a trilayer heterostructure of graphene/PTCDI/TiOPc, where the spatial separation of photoexcited electrons and holes in graphene and TiOPc, respectively, leads to the formation of long-lived photoexcitations with a lifetime of approximately 500 ps. Furthermore, spatially resolved transient absorption measurements reveal the immobile nature of these excitations, confirming that they are charge-transfer excitons rather than free electrons and holes. These results provide valuable insights into the complex interlayer photoexcitation transfer properties and demonstrate precise control over layer population and the recombination lifetime of photocarriers in such hybrid heterostructures.

Introduction

Organic materials have garnered significant interest due to their diverse applications and ease of large-scale deposition for industrial purposes. These materials can be readily grown on various substrates using a range of vapor or solution deposition techniques.[1–7] Notably, their compatibility with flexible substrates enables the development of bendable and foldable electronic and optoelectronic devices.[8–10] The low-cost manufacturing of organic thin films makes them highly desirable as cost-effective alternatives to traditional inorganic semiconductors. Furthermore, organic materials offer extensive opportunities for tuning their optical

and electronic properties through molecular design.[11,12]

Hybrid van der Waals heterostructures, created by combining organic and inorganic materials, have the potential to integrate the unique properties of both, enabling the development of novel artificial materials for a wide range of applications.[13,14] For instance, organic semiconductors typically exhibit high and wavelength-tunable light absorption and emission capabilities but often have poorer charge transport properties compared to their inorganic counterparts. By combining organic and inorganic semiconductors, it is possible to create functional materials with enhanced optical and transport properties.

In van der Waals heterostructures, interlayer charge and energy transfer play a crucial role in integrating the properties of individual materials and exploiting their emergent characteristics. In inorganic heterostructures, charge and energy transfer typically dominate at type-II and type-I interfaces, respectively.[15] However, in hybrid heterostructures, the low dielectric constant of the organic layers and the large binding energies of intralayer and charge-transfer excitons often complicate excitation transfer pathways.

In this work, we demonstrate that while perylenetetracarboxylic diimide (PTCDI) and titanyl phthalocyanine (TiOPc)—two prototype organic semiconductors—form a type-II interface characterized by charge-transfer exciton formation, their type-I interfaces with graphene exhibit distinct excitation transfer properties. Unlike the TiOPc/graphene interface, where energy transfer is the dominant mechanism, the PTCDI/graphene interface facilitates electron-hole separation by allowing electron transfer while preventing hole transfer. This unique feature, attributed to the band bending effects arising from ground-state charge transfer at the interface, enables the generation of long-lived charge-transfer excitons in the graphene/TiOPc/PTCDI trilayer heterostructure. These findings provide valuable insights into the excitation transfer processes at van der Waals organic/inorganic interfaces, paving the way for the design of hybrid artificial materials with tailored optoelectronic properties.

Methods

Sample Fabrication. The graphene was obtained via chemical vapor deposition (CVD), acquired from ACS Materials. It was transferred onto a quartz substrate and pre-cleaned by the vendor using the standard PMMA method. To ensure the cleanliness of the graphene surface, the graphene was annealed at $\sim$ 400°C overnight in an ultra-high vacuum (UVH) chamber with a base pressure of $\sim 10^{-9}$ Torr before organic molecule deposition. PTCDI and TiOPc molecules (sublimed, >99%) were acquired from Luminescence Technology (Taiwan), and they were used as-is. The PTCDI and TiOPc layers were deposited using the thermal evaporation technique, where powdered organic molecules are heated in crucibles to their sublimation point, allowing them to deposit onto the substrate. The thickness of the deposited layers was precisely monitored using a quartz crystal microbalance. The materials were deposited at a rate of $\sim$0.7–1.0 Å/min with the substrate at room temperature. For comparison, several control samples were also fabricated with the same technique, including standalone materials of Gr, PTCDI (2 nm), TiOPc (2 nm), and three bilayer heterostructures of Gr/PTCDI, Gr/TiOPc, and PTCDI/TiOPc.

Steady-State Spectroscopy. The PL spectroscopy was performed with a homemade setup with a 405-nm continuous-wave diode laser (Thorlabs) as the excitation source. With a 100 × and numerical aperature 0.75 objective lens, the focused laser spot size was about 1 μm. The PL was collected by the same objective lens and was sent to a spectrometer (Horiba iHR550) equipped with a thermoelectrically cooled CCD camera (Synapse). The absorption spectra were obtained by using a Perkin-Elmer spectrophotometer (Lambda 35 UV/Vis system, with an integrating sphere).

Transient Absorption Spectroscopy and Microscopy. Transient absorption measurements were performed with a homemade setup, which is based on a laser system including an 80 MHz and 100-fs Ti:sapphire oscillator and a photonic-crystal fiber supercontinuum generator. The Ti:sapphire oscillator is tuned to 750 nm. Part of this output was used as the probe directly. The rest of it is used to generate supercontinuum. A band pass filter at 580

nm with a band width of 10 nm was used to select a 580-nm pulse from the supercontinuum, serving as the pump pulse. The pump and probe pulses were combined by a beamsplitter and were co-focused on the sample to spot sizes of 1 - 2 μm by an objective lens. A mechanical chopper was used to modulate the pump intensity at about 3 KHz. The reflected probe is collimated by the focusing objective lens and measured by a silicon photodiode and a lock-in amplifier. For transient absorption measurements, the differential reflectance of the sample is measured by the probe as a function of the time delay between the pump and probe pulses. This differential reflectance is defined as $\Delta R/R_0 = (R - R_0)/R_0$, where R and R_0 are the reflectances of the sample with and without the presence of the pump beam, respectively. For transient absorption microscopy measurements, the probe spot is scanned across the pump spot by tilting a mirror in the probe arm. Time-resoved differential reflectance is recorded at each probe position, producing the spatiotemporally resolved differential reflectance data.

Density Functional Theory. In the DFT calculations, the exchange–correlation functional used the Perdew–Burke–Ernzerhof (PBE) parameterization of the generalized gradient approximation.[16] The plane-wave cutoff energy is 90 Ry. A k-point sampling of 2×2 is used for the Gr/PTCDI heterostructure with an in-plane unit cell size of 18.57 Å $\times$ 15.35 Å. The vacuum region is larger than 21 Å. Convergences of total and electronic energies are 10^{-5} eV/atom and 10^{-7} eV, respectively.

Results and Discussion

Sample Design and Absorption Spectroscopy. We constructed a trilayer hybrid heterostructure consisting of monolayer graphene (Gr), a 2-nm layer of PTCDI, and a 2-nm layer of TiOPc (see Methods), as schematically shown in Figure 1(a). The band alignment and our hypothesis on the photocarrier dynamics are summarized in Figure 1(b), where the Dirac cone near the K point of graphene is schematically plotted alongside the highest occupied molecular orbital (HOMO) and the lowest unoccupied molecular orbital (LUMO)

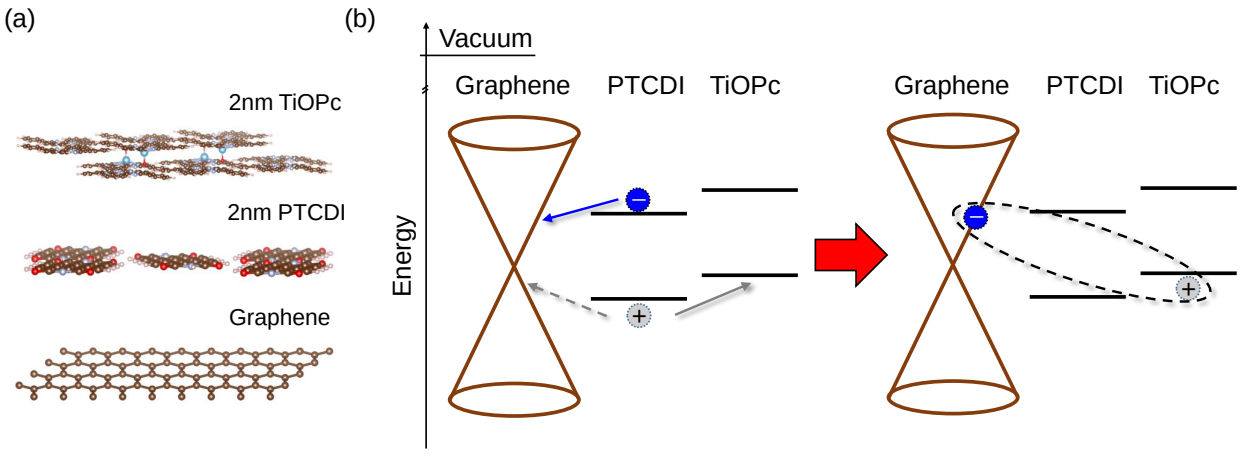

Figure 1: (a) Schematics of the heterostructure graphene/PTCDI/TiOPc (b) Band alignment and hypothesized photocarrier dynamics. Once excited in PTCDI, the holes and electrons transfer to TiOPc and graphene, respectively, resulting in the formation of charge-transfer excitons.

levels of PTCDI and TiOPc. It is well-known that PTCDI is an electron acceptor that can form a type-II heterojunction with phthalocyanine molecules,[17] while PTCDI and graphene form a type-I junction. Our hypothesis is that the photoexcited electrons and holes in PTCDI transfer to the graphene and TiOPc layers, respectively, forming charge-transfer excitons with a long recombination lifetime due to the separation of the electron and hole wavefunctions, as illustrated in Figure 1(b).

Absorption spectroscopy was performed to probe the available absorption bands of the organic semiconductors (see Methods). Figure 2 shows the absorption spectra of a set of samples, including Gr/PTCDI/TiOPc, Gr/TiOPc, Gr/PTCDI, and PTCDI. The green curves show two absorption peaks near 480 nm and 580 nm for PTCDI. In the Gr/PTCDI heterostructure, the 480-nm peak shifts to 520 nm, while the 580-nm peak remains unchanged. The red curve shows a TiOPc absorption peak near 750 nm. In the Gr/PTCDI/TiOPc heterostructure (black curve), both TiOPc and PTCDI peaks are observed.

Interlayer Charge Transfer Dynamics. Transient absorption measurements were performed to probe the photocarrier dynamics (see Methods). We selectively excite the PTCDI layer by tuning the pump to 580 nm (2.14 eV), one of its absorption peaks as shown

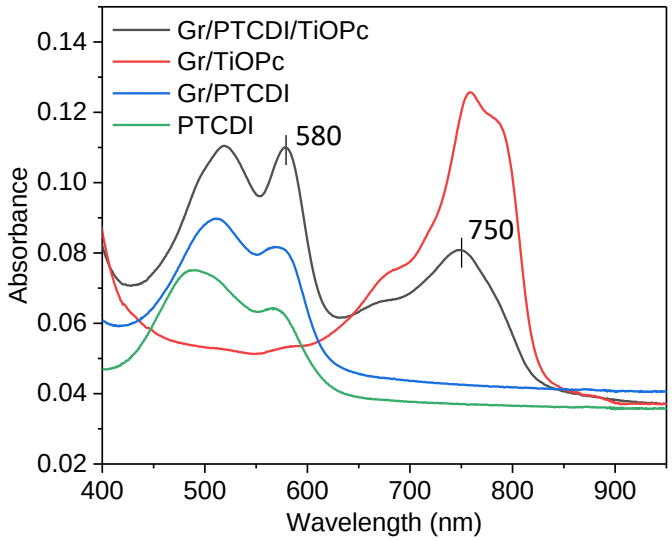

Figure 2: Absorption spectra of the Gr/PTCDI/TiOPc trilayer heterostructure and control samples.

in Figure 2, with a pulse energy fluence of 4.2 μJ cm^{-2}. The probe, with a fluence of 20 μJ cm^{-2}, is tuned to the TiOPc absorption peak at 750 nm (1.65 eV) to probe carrier transfer into TiOPc. The probe is also expected to be sensitive to carriers in graphene, which has no bandgap. The differential reflectance, $\Delta R/R_0 = (R - R_0)/R_0$, where R and R_0 are the sample reflectance with and without the pump, respectively, is measured as a function of the probe delay, which is the arrival time of the probe pulse at the sample with respect to the pump pulse.

Figure 3 shows the measured differential reflectance from the trilayer heterostructure, Gr/PTCDI/TiOPc, in comparison with that from samples of PTCDI, Gr/PTCDI, and PTCDI/TiOPc at long (a) and short (b) delays. To analyze the carrier dynamics in these heterostructures, we start with the signal from the PTCDI sample (green curves). The observed signal indicates that the 750-nm (1.65-eV) probe, intended to detect carriers in TiOPc, is also sensitive to carriers in PTCDI. We observe two decay processes with time constants $\tau_1 = 9.0 \pm 0.5$ ps and $\tau_2 = 250 \pm 60$ ps. We attribute the fast decay, τ_1, to either the fast recombination of electrons and holes by traps or exciton formation, while the slow decay process of τ_2 can be attributed to exciton lifetime in PTCDI.[18]

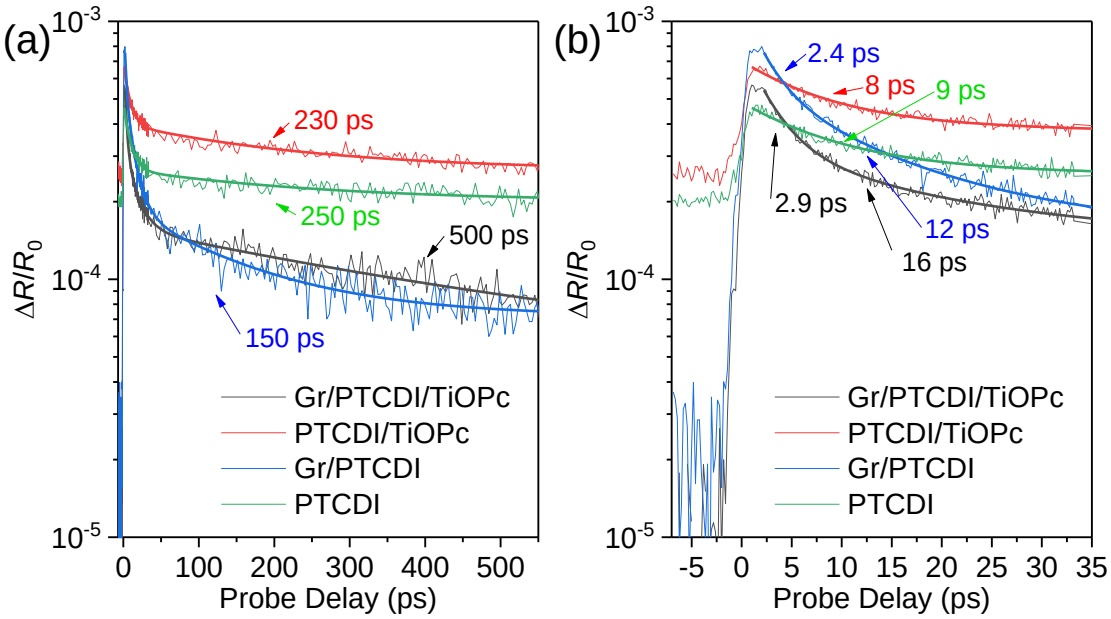

Figure 3: (a) Time-dependent differential reflectance of a 1.65-eV probe with the 2.14-eV pump pulse for the trilayer heterostructure and other control samples. The solid curves are bi-exponential and tri-exponential fits for samples without graphene and with graphene, respectively. Long-lived decay processes are labeled. (b) Same as (a) zooming in on early probe delays with short-lived decay processes labeled.

As shown by the red curves, the signal from the PTCDI/TiOPc heterostructure is about 1.5 times larger than that of PTCDI. Since PTCDI and TiOPc form a type-II interface, holes excited in PTCDI could transfer to TiOPc. Because the probe is tuned to the TiOPc absorption peak, the hole transfer to TiOPc is expected to enhance the signal, which is consistent with the data. Indeed, since TiOPc is not photoexcited (confirmed by the lack of signal from the TiOPc sample, Figure S1) and the electrons excited in PTCDI cannot transfer to TiOPc, the signal from the PTCDI/TiOPc heterostructure would have had the same magnitude without hole transfer to TiOPc. The signal also decays bi-exponentially, with similar decay time constants of 8 and 230 ps. We assign the slow time constant to the lifetime of charge-transfer excitons formed by the transferred holes in TiOPC and electrons that reside in PTCDI.

We now compare the signal from the Gr/PTCDI heterostructure with that of PTCDI. The differential reflectance from Gr/PTCDI is twice as large and decays tri-exponentially

with three time constants of 2.4, 12, and 150 ps. The 2.4-ps process can be assigned to photocarriers that are directly excited and recombine in graphene, since this time scale matches the photocarrier lifetime in graphene (Figure S1). The intermediate process, a 12-ps decay, is caused by recombination or exciton formation in PTCDI, as in the case of PTCDI alone.

The 150-ps process is the most interesting observation: Graphene and PTCDI form a type-I band alignment, with the Dirac point of graphene residing between the HOMO and LUMO levels of PTCDI. In a typical type-I interface, one would expect most electrons and holes photoexcited in the wider-gap layer to transfer into the narrower-gap layer and recombine. Since the carrier recombination lifetime in graphene is very short, if the transfer pathway is efficient for both electrons and holes, the overall lifetime of these carriers would be on the order of a few ps. Indeed, such ultrashort dynamics was observed in the type-I heterostructure of Gr/TiOPc (Figure S1). Hence, the observation of the lifetime as long as 150 ps rules out this possibility. On the other hand, if neither electrons nor holes transfer to graphene, the signal from Gr/PTCDI would resemble that of PTCDI, except for the additional 2.4-ps component from graphene, which contradicts the data. Therefore, we conclude that, despite the type-I interface, only one type of carrier—electrons or holes—transfers to graphene. This is supported and explained by density functional theory (DFT) calculations on the interface coupling, details of which will be discussed later. The 150-ps process is thus associated with the lifetime of charge-transfer excitons across the Gr/PTCDI interface.

The signal from the trilayer heterostructure of Gr/PTCDI/TiOPc (black curves) provides strong evidence to identify electrons as the transferred carriers. We observed a fast recombination of 2.9-ps, attributed to graphene, followed by an intermediate process of 16 ps and a very slow process of 500 ps. The 500-ps process is much slower than the decays observed in any of the other heterostructures. If the holes, instead of electrons, were to transfer to graphene, the trilayer heterostructure would form two types of previously observed charge-

transfer excitons: those formed by electrons in PTCDI and holes in graphene (with a lifetime of 150 ps) and those formed by electrons in PTCDI and holes in TiOPc (230 ps). The 500-ps lifetime is longer than both. Therefore, the only plausible scenario is that electrons transfer to graphene and form charge-transfer excitons with the holes that transferred to TiOPc. Since the electrons and holes are spatially separated by PTCDI, such excitons naturally exhibit a longer lifetime. Our previous optoelectrical measurements also show that optical excitation of similar trilayer structures can lead to electron injection into graphene.[19,20]

In these exponential fits, a constant offset was included to account for a time-independent component of the signal, as evidenced by the nonzero signal observed at negative probe delays [Figure 3(b)]. This component increases with pump fluence [Figure S2(a)] and is attributed to the cumulative thermal effect of previous pump pulses. However, this offset does not affect our analysis of the time-resolved signal generated by photocarriers excited by the present pump pulse.

Photoluminescence (PL) spectroscopy is further used to confirm the above interpretation (see Methods). The blue curve in Figure 4 is the PL spectrum from a 2-nm PTCDI deposited on hBN under the excitation of 405-nm continuous-wave laser. The three peaks of PTCDI are significantly quenched by about 200-300 times in the PTCDI/TiOPc heterostructure (red curve), due to the transfer of the holes that are excited in PTCDI and then transfered to TiOPc. A small PL peak near 800 nm is from TiOPc. As shown by the black curve, the recombination pathway present in PTCDI/TiOPc is highly quenched in Gr/PTCDI/TiOPc, indicating efficient charge transfer from PTCDI into graphene. Since we have established that holes in PTCDI efficiently transfer to TiOPc, the significant additional quenching of PTCDI peaks can be attributed to electron transfer to graphene. The peak near 800 nm is still present in the trilayer heterostructure. The lack of quenching of this peak indicates that the recombination in TiOPc, which is not in contact with graphene, is less affected. A new peak near 940 nm appears in the trilayer heterostructure, suggesting that an intermediate, lower-energy recombination pathway is introduced by graphene. This peak could be assigned

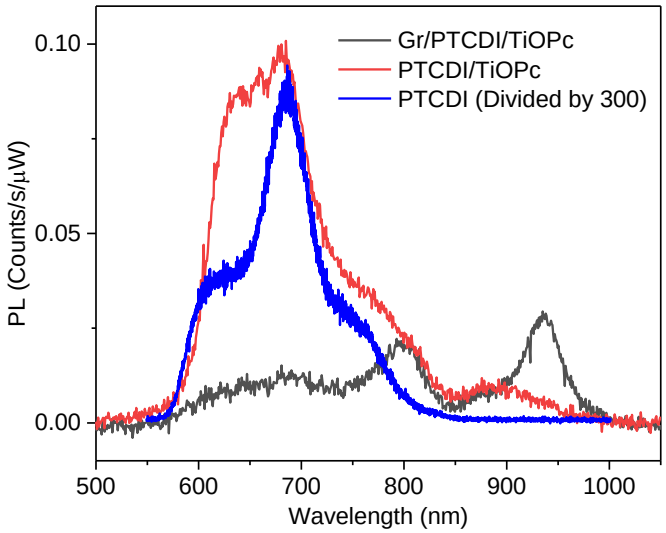

Figure 4: Photoluminescence spectra of PTCDI (blue, divided by 300), PTCDI/TiOPc (red), and Gr/PTCDI/TiOPc (black) measured under the same conditions.

to the long-lived charge-transfer excitons with electrons and holes in graphene and TiOPc, respectively, although more studies are necessary to fully understand this feature.

Band Bending and electron transfer at Gr/PTCDI Interface by DFT. To reveal the physical mechanisms on the different transfer properties of electrons and holes at the presumed type-I interface of Gr/PTCDI, first-principles calculations based on the DFT were performed using the Quantum Espresso package[21,22] with the optimized norm-conserving Vanderbilt pseudopotentials[23] from the PseudoDojo library (see Methods).[24]

The atomic structure of a PTCDI molecular layer on graphene is shown in Figure 5(a), which features a unit cell with parameters $a = 15.35$Å, $b = 18.57$Å, and $\gamma = 97.3°$, in good agreement with STM observations.[25] To better understand the interface excitons and charge transfer, we calculated the band structure and ground-state charge transfer for the Gr/PTCDI heterostructure, as shown in Figures 5(b-c). The projected band structure in Figure 5(b), with dark purple and yellow representing graphene and PTCDI contributions, respectively, reveals strong interface electronic coupling for Gr/PTCDI. The significant hybridization of the LUMO of PTCDI and the graphene low-energy bands near the Fermi level facilitates efficient excited-state electron transfer, which is in agreement with the ul-

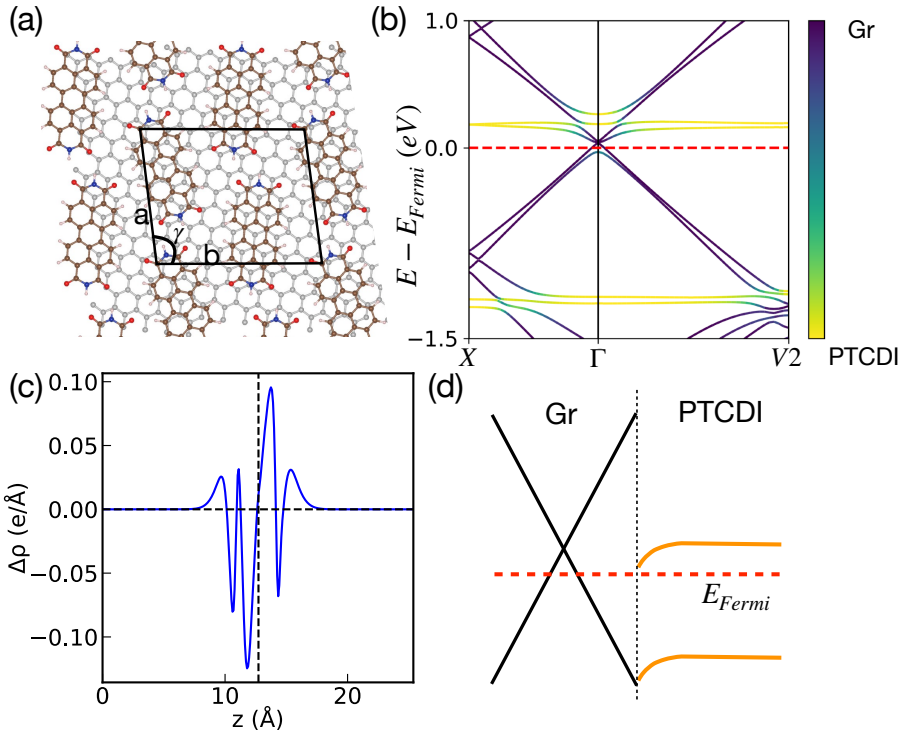

Figure 5: (a) Atomic structure of PTCDI/graphene. The unit cell parameters are $a = 15.35$ Å, $b = 18.57$ Å, and $\gamma = 97.3°$. (b) Projected band structure: the dark purple and yellow regions represent contributions from graphene and PTCDI, respectively. (c) Charge density redistribution ($\Delta\rho$) along the z-direction, with the dashed vertical line indicating the position of the interface—graphene on the left and PTCDI on the right. (d) Schematic illustrating band bending resulting from ground-state electron transfer from graphene to PTCDI.

trafast dynamics observed for Gr/PTCDI. On the contrary, the LUMO is far below the Fermi level, through hybridization with the occupied electronic states of graphene, the hole transfer from PTCDI to graphene is less efficient. The downshift of the Fermi level below the graphene Dirac point indicates ground-state charge transfer from graphene to the PTCDI molecules. This is further supported by the electron density redistribution $\Delta\rho$ at the interface, as shown in Figure 5(c), where $\Delta\rho = \rho[\text{Gr/PTCDI}] - \rho[\text{Gr}] - \rho[\text{PTCDI}]$. The integrated electron transfer amounts to approximately 0.098 electrons per PTCDI molecule. This ground-state charge transfer from graphene to PTCDI leads to downward band bending of the HOMO and LUMO at the interface, schematically illustrated in Figure 5(d). Therefore, in addition to the LUMO energy being far below the Fermi level, this downward band

bending increases the energy barrier for excited hole transfer. This explains the formation of the charge-transfer excitons in Gr/PTCDI and Gr/PTCDI/TiOPc with the absence of excited hole transfer from PTCDI to graphene.

In-Plane Transport to Identify Nature of Photocarriers. We have established the separation of electrons and holes in the Gr/PTCDI/TiOPc heterostructure and hypothesized that they form charge-transfer excitons, rather than non-interacting and freely moving charge carriers. One way to test this hypothesis is to study their in-plane transport properties. If the electrons in graphene are free carriers, they should exhibit a rather large mobility. On the other hand, if the electrons are bound to the holes in TiOPc to form excitons, they would be largely immobile due to the low mobility of holes in TiOPc.

The in-plane transport of the photocarriers in Gr/PTCDI/TiOPc was studied by spatiotemporally transient absorption microscopy measurements with 2.14-eV and 4.2 μJ cm^{-2} pump and 1.65-eV and 20 μJ cm^{-2} probe pulses, respectively (see Methods). A power-dependent measurement confirms that with this pump fluence, the signal is approximately proportional to the carrier density (Figure S2). In the spatiotemporally resolved measurements, the probe spot is scanned across the pump spot. At each position, the time-dependent differential reflectance signal is recorded and compiled into Figures 6(a), (d), and (g), showing the early, middle, and late stages of time development. Figures 6(b), (e), and (h) present examples of the spatial profiles of the signal at various probe delays as labeled. Each measured profile is fit by a Gaussian function. The deduced variance, σ^2, is then plotted in Figures 6(c), (f), and (i) to reveal potential broadening of the profile. If carriers diffuse in-plane, the variance of their distribution increases linearly as $\sigma^2(t) - \sigma_0^2 = 2Dt$, where D is the diffusion coefficient.[26]

We observed a trend of broadening of the profiles at very early delays near 1 ps in Figure 6(c), indicative of carrier diffusion. A linear fit reveals a diffusion coefficient of 105 cm^2 s^{-1}. Using Einstein's relation, we calculated a mobility of about $\mu = 8100$ cm^2 V^{-1} s^{-1}. This mobility is robust and reproducible across multiple scans at different sample locations, and is

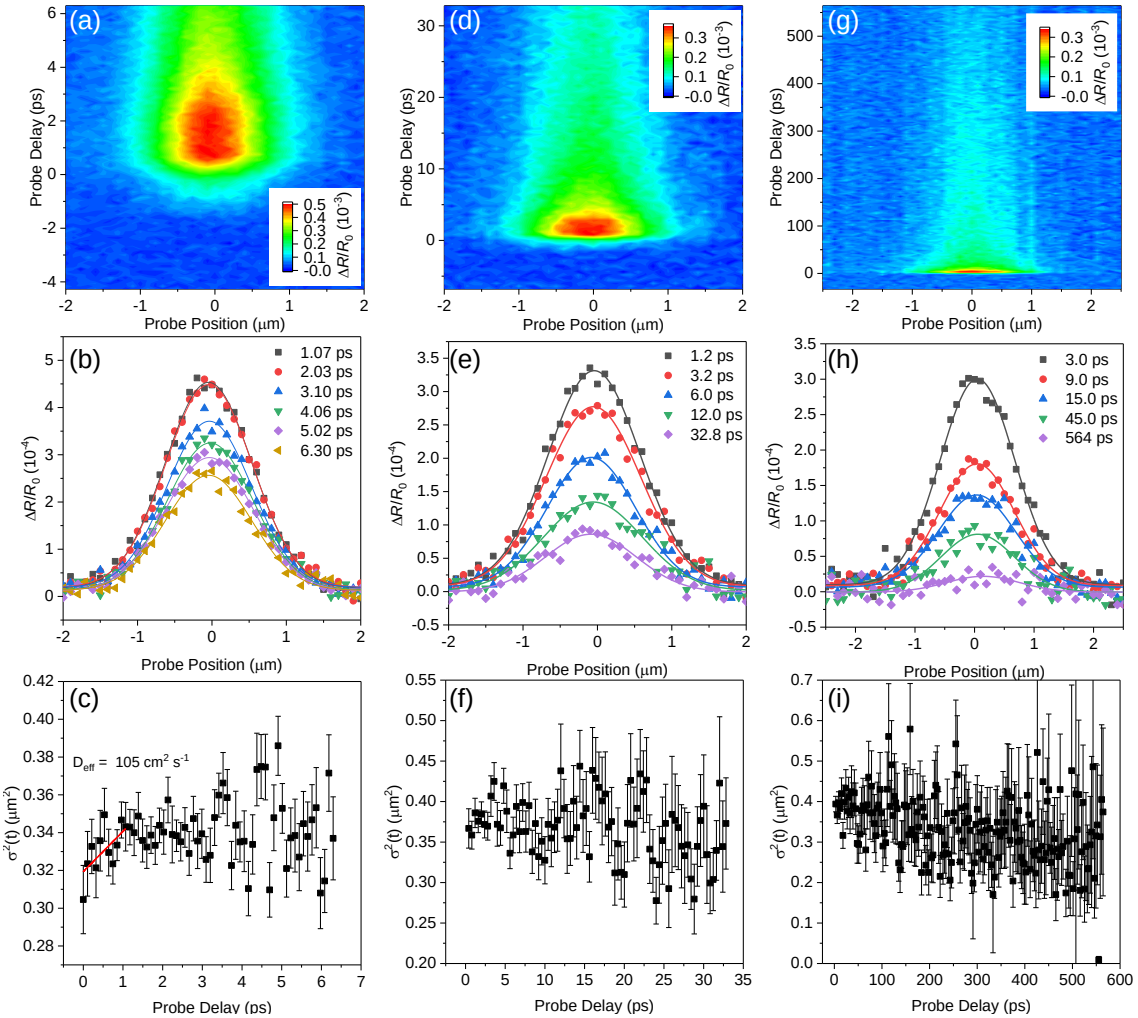

Figure 6: (a) Spatiotemporally resolved differential reflectance with a 2.14-eV pump and a 1.65-eV probe at short delays near the peak from the trilayer heterostructure of Gr/PTCDI/TiOPc. (b) Examples of the spatial profiles shown in (a) at various probe delays and the corresponding Gaussian fits (curves). (c) The variance of the profiles shown in (a) as a function of probe delay. The red line is a linear fit for the fast, sub-ps process. (d-f) and (g-i) Same as (a-c) showing mid-range and long-range decay processes, respectively.

consistent with previous results for carrier mobility in CVD graphene.[26] This high mobility is thus attributed to the electrons and holes directly excited in graphene by the pump, which recombine on a 1-ps timescale (Figure S1).

After this very fast initial diffusion, the signal primarily arises from the transferred electrons and holes from PTCDI to graphene and TiOPc, respectively. These photocarriers remain stagnant, as indicated by a relatively flat variance in Figures 6(c), (f), and (i). The

absence of statistically significant broadening of the profiles after 1 ps indicates the ultralow mobility of these carriers, confirming their nature as charge-transfer excitons. Organic semiconductors often exhibit very low mobilities; for example, PTCDI has a reported mobility on the order of 0.1 $cm^2\ V^{-1}\ s^{-1}$.[27] This mobility corresponds to a diffusion coefficient of 0.003 $cm^2\ s^{-1}$ and an increase of the variance, $\sigma^2(t) - \sigma_0^2$, of $3 \times 10^{-4}\ \mu m^2$ at $t = 500$ ps, which is within the noise level of our data.

Conclusions

We have fabricated bilayer and trilayer heterostructures by combining graphene, PTCDI, and TiOPc, and studied their photocarrier dynamics using absorption and PL spectroscopy, transient absorption spectroscopy, transient absorption microscopy, and DFT calculations. Our findings confirm that the two organic materials form a type-II interface, characterized by the formation of charge-transfer excitons, with electrons residing in PTCDI and holes in TiOPc. TiOPc forms a type-I heterostructure with graphene, as evidenced by the ultrafast transfer of electrons and holes to graphene, followed by their rapid recombination within graphene. Although the PTCDI/graphene interface exhibits type-I behavior, our experiments revealed that only electrons transfer from PTCDI to graphene, with no observable hole transfer. DFT calculations demonstrate a ground-state electron transfer of approximately 0.1 electrons per molecule from graphene to PTCDI, shifting the graphene Fermi level below its Dirac point. The resulting p-type doping of graphene and n-type doping of PTCDI create a built-in electric field at the interface, inducing band bending that prevents excited holes from transferring from PTCDI to graphene. This phenomenon is exploited in the Gr/PTCDI/TiOPc trilayer heterostructure, where spatial separation of electrons and holes results in the formation of long-lived and immobile charge-transfer exciton with a lifetime of approximately 500 ps. These results offer valuable insights into the complex interlayer photoexcitation transfer mechanisms in van der Waals heterostructures and demonstrate precise control over layer

population and photocarrier recombination lifetimes in hybrid materials.

Acknowledgement

This work is primarily supported by US National Science Foundation Award No. DMR-2401141. H.Z. is supported by the U.S. Department of Energy, Office of Basic Energy Sciences, Division of Materials Sciences and Engineering under Award No. DE-SC0020995. R.J.S. acknowledges support by Redeker Fellowship and Ralston Fellowship. A.S and Q.Z. acknowledge the computational resources at Argonne National Laboratory and the Pittsburgh Supercomputing Center. Work performed at the Center for Nanoscale Materials, a U.S. Department of Energy Office of Science User Facility, was supported by the U.S. DOE, Office of Basic Energy Sciences, under Contract No. DE-AC02-06CH11357. This work used Bridges-2 at the Pittsburgh Supercomputing Center through allocation PHY230195 from the Advanced Cyberinfrastructure Coordination Ecosystem: Services & Support (ACCESS) program, which is supported by U.S. National Science Foundation grants Nos. 2138259, 2138286, 2138307, 2137603, and 2138296.

Supporting Information Available

Additional differential reflectance data of graphene and Gr/TiOPc, power-dependent differential reflectance of Gr/PTCDI/TiOPc.

References

(1) Vasseur, K.; Rolin, C.; Vandezande, S.; Temst, K.; Froyen, L.; Heremans, P. A Growth and Morphology Study of Organic Vapor Phase Deposited Perylene Diimide Thin Films for Transistor Applications. *J. Phys. Chem. C* **2010**, *114*, 2730–2737.

(2) Bagchi, K.; Ediger, M. D. Controlling Structure and Properties of Vapor-Deposited

Glasses of Organic Semiconductors: Recent Advances and Challenges. *J. Phys. Chem. Letters* **2020**, *11*, 6935–6945.

(3) Ruiz, R.; Choudhary, D.; Nickel, B.; Toccoli, T.; Chang, K.-C.; Mayer, A. C.; Clancy, P.; Blakely, J. M.; Headrick, R. L.; Iannotta, S. et al. Pentacene Thin Film Growth. *Chem. Mater.* **2004**, *16*, 4497–4508.

(4) Virkar, A. A.; Mannsfeld, S.; Bao, Z.; Stingelin, N. Organic Semiconductor Growth and Morphology Considerations for Organic Thin-Film Transistors. *Adv. Mater.* **2010**, *22*, 3857–3875.

(5) Dimitrakopoulos, C. D.; Mascaro, D. J. Organic thin-film transistors: A review of recent advances. *IBM J. Res. Develop.* **2001**, *45*, 11–27.

(6) Chang, P.; Molesa, S.; Murphy, A.; Frechet, J.; Subramanian, V. Inkjetted crystalline single monolayer oligothiophene OTFTs. *IEEE Trans. Elec. Dev.* **2006**, *53*, 594–600.

(7) Dimitrakopoulos, C.; Malenfant, P. Organic Thin Film Transistors for Large Area Electronics. *Adv. Mater.* **2002**, *14*, 99–117.

(8) Sawatzki-Park, M.; Wang, S.-J.; Kleemann, H.; Leo, K. Highly Ordered Small Molecule Organic Semiconductor Thin-Films Enabling Complex, High-Performance Multi-Junction Devices. *Chem. Rev.* **2023**, *123*, 8232–8250.

(9) Zschieschang, U.; Waizmann, U.; Weis, J.; Borchert, J. W.; Klauk, H. Nanoscale flexible organic thin-film transistors. *Sci. Adv.* **2022**, *8*, eabm9845.

(10) Fujisaki, Y.; Koga, H.; Nakajima, Y.; Nakata, M.; Tsuji, H.; Yamamoto, T.; Kurita, T.; Nogi, M.; Shimidzu, N. Transparent Nanopaper-Based Flexible Organic Thin-Film Transistor Array. *Adv. Funct. Mater.* **2013**, *24*, 1657–1663.

(11) Guo, X.; Xu, Y.; Ogier, S.; Ng, T. N.; Caironi, M.; Perinot, A.; Li, L.; Zhao, J.;

Tang, W.; Sporea, R. A. et al. Current Status and Opportunities of Organic Thin-Film Transistor Technologies. *IEEE Trans. Elec. Dev.* **2017**, *64*, 1906–1921.

(12) Azarova, N. A.; Owen, J. W.; McLellan, C. A.; Grimminger, M. A.; Chapman, E. K.; Anthony, J. E.; Jurchescu, O. D. Fabrication of organic thin-film transistors by spray-deposition for low-cost, large-area electronics. *Org. Elec.* **2010**, *11*, 1960–1965.

(13) Huang, X.; Tan, C.; Yin, Z.; Zhang, H. 25th Anniversary Article: Hybrid Nanostructures Based on Two-Dimensional Nanomaterials. *Adv. Mater.* **2014**, *26*, 2185–2204.

(14) Jariwala, D.; Marks, T. J.; Hersam, M. C. Mixed-Dimensional van Der Waals Heterostructures. *Nat. Mater.* **2017**, *16*, 170.

(15) Jin, C. H.; Ma, E. Y.; Karni, O.; Regan, E. C.; Wang, F.; Heinz, T. F. Ultrafast Dynamics in van der Waals Heterostructures. *Nat. Nanotechnol.* **2018**, *13*, 994–1003.

(16) Perdew, J. P.; Burke, K.; Ernzerhof, M. Generalized Gradient Approximation Made Simple. *Phys. Rev. Lett.* **1996**, *77*, 3865–3868.

(17) Kahn, A.; Koch, N.; Gao, W. Electronic structure and electrical properties of interfaces between metals and π-conjugated molecular films. *J. Polym. Sci. Part B: Polym. Phys.* **2003**, *41*, 2529–2548.

(18) Yoshida, T.; Watanabe, K. Spectral Diffusion of Excitons in 3, 4, 9, 10-Perylenetetracarboxylic-diimide (PTCDI) Thin Films. *J. Phys. Chem. B* **2021**, *125*, 9350–9356.

(19) Wanigasekara, S.; Kattel, B.; Rudayni, F.; Chan, W.-L. Extracting Electrons from Delocalized Excitons by Flattening the Energetic Pathway for Charge Separation. *J. Phys. Chem. Lett.* **2021**, *12*, 9047–9054.

(20) Wanigasekara, S.; Rijal, K.; Rudayni, F.; Panth, M.; Shultz, A.; Wu, J. Z.; Chan, W.-L. Using an Atomically Thin Layer of Hexagonal Boron Nitride to Separate Bound Charge-Transfer Excitons at Organic Interfaces. *Phys. Rev. Appl.* **2022**, *18*, 014042.

(21) Giannozzi, P.; Baroni, S.; Bonini, N.; Calandra, M.; Car, R.; Cavazzoni, C.; Ceresoli, D.; Chiarotti, G. L.; Cococcioni, M.; Dabo, I. et al. QUANTUM ESPRESSO: A Modular and Open-Source Software Project for Quantum Simulations of Materials. *J Phys.: Condens. Mat.* **2009**, *21*, 395502.

(22) Giannozzi, P.; Andreussi, O.; Brumme, T.; Bunau, O.; Buongiorno Nardelli, M.; Calandra, M.; Car, R.; Cavazzoni, C.; Ceresoli, D.; Cococcioni, M. et al. Advanced capabilities for materials modelling with Quantum ESPRESSO. *J Phys.: Condens. Mat.* **2017**, *29*, 465901.

(23) Hamann, D. R. Optimized norm-conserving Vanderbilt pseudopotentials. *Phys. Rev. B* **2013**, *88*, 085117.

(24) van Setten, M.; Giantomassi, M.; Bousquet, E.; Verstraete, M.; Hamann, D.; Gonze, X.; Rignanese, G.-M. The PseudoDojo: Training and grading a 85 element optimized norm-conserving pseudopotential table. *Comput. Phys. Commun.* **2018**, *226*, 39–54.

(25) Karmel, H. J.; Garramone, J. J.; Emery, J. D.; Kewalramani, S.; Bedzyk, M. J.; Hersam, M. C. Self-assembled organic monolayers on epitaxial graphene with enhanced structural and thermal stability. *Chem. Commun.* **2014**, *50*, 8852–8855.

(26) Scott, R. J.; Valencia-Acuna, P.; Zhao, H. Spatiotemporal Observation of Quasi-Ballistic Transport of Electrons in Graphene. *ACS Nano* **2023**, *17*, 25368–25376.

(27) Balambiga, B.; Dheepika, R.; Devibala, P.; Imran, P. M.; Nagarajan, S. Picene and PTCDI based Solution Processable Ambipolar OFETs. *Sci. Rep.* **2020**, *10*, 22029.

TOC Graphic